Cell. Mol. Biol. (ISSN: 1165-158X)

Journal Homepage: www.cellmolbiol.org

Cellular and Molecular Biology

Original Article

Molecular insights into the interaction of *Coptis teeta* protoberberine alkaloids with human topoisomerase 1B-DNA complex: an integrated computational study

Jagadish Babu Dasari[1*], Mahesh Babu Dasari[2], Aparna Chimalamari[1], Syed Junied[1], Bini Chhetri Soren[1]

[1] *Department of Research and Development, Quanton Biolife Sciences, Ghatsila, Jharkhand, India*
[2] *Department of Artificial Intelligence, University of Texas, Austin, USA*

Article Info

Article history:

Received: January 19, 2026
Accepted: April 02, 2026
Published: April 30, 2026

Use your device to scan and read the article online

Abstract

Human topoisomerase 1B (hTopo1B) is a validated anticancer target due to its key role in relieving torsional stress during DNA replication and transcription, as well as its overexpression in rapidly proliferating tumor cells. Camptothecin (CPT) and its derivatives are principal hTopo1B-targeting agents but face challenges including lactone ring instability, dose-limiting toxicities, and acquired drug resistance. This research investigated seven protoberberine alkaloids from *Coptis teeta* alkaloids-berberine, coptisine, epiberberine, berberastine, jatrorrhizine, palmatine, and fetidine as potential CPT-like hTopo1B inhibitors using comprehensive computational methods. Density functional theory (DFT) calculations showed that six of the seven alkaloids had HOMO-LUMO gaps (2.608-3.015 eV) and electrophilicity indices similar to CPT, suggesting a capacity for charge transfer and DNA intercalation. Molecular docking of the hTopo1B-DNA binary complex (PDB:1A36) revealed that all compounds stabilized the covalent cleavage complex through π-π stacking and hydrogen bonds at the scissile site, with coptisine and epiberberine showing the strongest binding affinities (−10.32 and −10.53 kcal/mol, respectively). Molecular dynamics simulations over 250 ns confirmed the structural stability of the complexes, with low RMSD and RMSF values and minimal fluctuations in the radius of gyration. MM/GBSA and MM/PBSA binding free energy analyses consistently ranked epiberberine as the strongest binder (ΔG = −18.86 and −14.12 kcal/mol), followed by berberine and coptisine. Per-residue decomposition identified key contacts with the DNA bases DT118, DA17, and DA14, as well as with the protein residues GLU179 and GLY201. All protoberberine analogs showed drug-likeness in ADME profiling, good oral availability, and no PAINS alerts. These findings suggest that protoberberine alkaloids from *C.teeta*, especially epiberberine, coptisine, and berberine, are promising candidates for next-generation hTopo1B-targeted anticancer therapeutics. Experimental validation is required to confirm the proposed mechanism.

Keywords: Human topoisomerase 1B, *Coptis teeta*, protoberberine alkaloids, molecular docking, molecular dynamics simulations.

1. Introduction

Cancer remains one of the leading causes of morbidity and mortality worldwide, driving the urgent need for novel therapeutic strategies and molecular targets [1]. Among the validated targets in anticancer drug discovery, human topoisomerase 1B (hTopo1B) has attracted considerable attention owing to its indispensable role in DNA replication, transcription, and cell division [2]. Htopo1B is a type 1B nuclear enzyme that relaxes torsional stress in duplex DNA by introducing transient single-strand breaks, allowing controlled rotation of the cleaved strand around the intact strand, followed by strand religation to restore DNA integrity. Given its preferential overexpression in rapidly proliferating tumor cells compared to normal tissues, hTopo1B represents an attractive target for selective anticancer interventions [3]. Camptothecin (CPT), a pentacyclic alkaloid originally isolated from *Camptotheca acuminata,* is a prototypical hTopo1B poison and serves as a paradigm for interfacial inhibitors. CPT and its clinical derivatives, topotecan and irinotecan, exert cytotoxicity by intercalating the protein-DNA interface within the hTopo1B-DNA binary complex, thereby stabilizing the covalent cleavage intermediate and preventing strand religation [4]. The resulting accumulation of irreversible DNA double-strand breaks during replication fork collision ultimately triggers apoptosis in rapidly dividing tumor cells [5]. Despite the established clinical utility of CPT-based drugs, their use is limited by the intrinsic instability of the lactone ring, dose-limiting toxicities, acquired drug resistance, and suboptimal pharmacokinetic profiles. This necessitates continued efforts to identify structurally novel hTopo1B-targeting scaffolds with improved therapeutic windows [6, 7].

Plant-derived alkaloids have historically been a rich source of bioactive scaffolds for anticancer drug discovery [8]. Among these, protoberberine alkaloids, a subclass of isoquinoline alkaloids characterized by a tetracyclic aro-

* Corresponding author.
E-mail address: drjagadishdasari@gmail.com; jagadish@qblsci.com (J. B. Dasari).
Doi: http://dx.doi.org/10.14715/cmb/2026.72.4.5

matic ring system, have demonstrated broad-spectrum biological activities, including antimicrobial, anti-inflammatory, antidiabetic, and cytotoxic effects [9] [10]. Berberine, the most extensively studied protoberberine alkaloid, has been shown to intercalate into DNA and inhibit topoisomerase activity, suggesting a potential mechanism of action similar to CPT [11]. Related structural analogs, including coptisine, epiberberine, berberastine, jatrorrhizine, and palmatine, share a planar quaternary nitrogen framework that is conducive to DNA intercalation; however, their interactions with the hTopo1B-DNA cleavage complex remain incompletely understood and poorly characterized at the molecular level [12].

Coptis teeta (Family: Ranunculaceae), also known as Mishmi tita or Indian goldthread, is a key medicinal herb native to the Himalayas, used in traditional Ayurvedic and Chinese medicine.

C.teeta rhizomes and roots are rich in protoberberine alkaloids, including berberine, coptisine, epiberberine, berberastine, jatrorrhizine, palmatine, and the structurally distinct fetidine. Ethnobotanical and phytochemical research indicates that these alkaloids exhibit cytotoxic and anticancer activity. However, the precise molecular mechanisms underlying their potential antitumor effects, particularly inhibition of hTopo1B, have not been systematically elucidated [13]. This study investigates the potential of *C. teeta* protoberberine alkaloids as novel hTopo1B-targeting agents, providing mechanistic insights for safer and more effective anticancer therapeutics.

2. Materials and Methods

2.1. Protein structure preparation

The crystal structure of the human topoisomerase 1B (hTopo1B)-DNA complex, lacking the N-terminal domain (residues 1-200), was retrieved from the Protein Data Bank (PDB ID: 1A36) for molecular docking. Camptothecin (CPT), bound in the original crystal structure, was removed from the complex using UCSF ChimeraX [14]. The protein was converted to PDBQT format using AutoDock Tools v4.2.6 [15]. During the preparation step, all non-standard residues, water molecules, and pre-bound ligands were deleted. Polar hydrogens and Gasteiger-Marsili charges were added. The final protein structure was saved as PDBQT format for molecular docking.

2.2. Ligand Preparation

Seven *Coptis teeta* derivatives were chosen and retrieved from the PubChem database in PDB format. Energy minimization and geometry optimization were performed using Avogadro version 2.0.6 [16]. Each ligand was prepared by merging nonpolar hydrogens, assigning Gasteiger-Marsili charges, and modifying atom types according to AutoDock specifications. Rotatable bonds were subsequently defined, and ligands were saved in PDBQT format using AutoDock Tools v4.2.6.

2.3. Density Functional Theory (DFT) analysis

The electronic properties of the seven chosen ligands were investigated using DFT calculations performed using ORCA quantum chemistry software (v6.1.1) [17]. IboView (v20211019-RevA) was used to prepare and visualize molecular structures and molecular orbitals. The geometry of all ligands was optimized using the Becke-Lee-Yang-Parr (BLYP) exchange-correlation functional with the def2-SVP basis set. Optimization was performed without symmetry constraints to ensure full relaxation of the molecular geometries. Standard ORCA convergence settings (NormalSCF, NormalGrid, and NormalPrint) were applied to obtain well-converged ground-state structures. Subsequently, single-point energy calculations and frontier molecular orbital analyses were performed using the B3LYP hybrid functional with a 6-31G(d) basis set. Frequency calculations at the B3LYP/6-31G(d) level confirmed that the optimized structures corresponded to true minima on the potential energy surface. The energies of the Highest Occupied Molecular Orbital (HOMO) and Lowest Unoccupied Molecular Orbital (LUMO) obtained from these calculations were used to compute conceptual DFT descriptors, including the HOMO-LUMO energy gap (ΔE), ionization potential (I), electron affinity (A), chemical hardness (η), electronegativity (χ), and electrophilicity index (ω), all calculated based on Koopmans' theorem, as shown in Fig.1 and Table.1.

2.4. Molecular docking analysis

Molecular docking simulations were performed using AutoDock Tools v4.2.6. The 2.80 Å X-ray crystallographic structure of the hTopo1B-DNA complex (1A36) was selected as the binding pocket for molecular docking studies. The stereochemical quality of the protein structure was evaluated using PROCHECK [18], and the Ramachandran plot analysis and residue distribution were presented in Fig. S2 and Table S2. The docking grid box was centered on the active site of the hTopo1B-DNA complex using AutoDock Tools v4.2.6. The binding site regions were mapped and defined using grid boxes with precisely determined x-, y-, and z-coordinates (Table S1). For each ligand, ten molecular docking simulations were performed, each consisting of ten docking runs. The optimal pose was selected based on the lowest binding energy score and visual inspection of ligand-protein interactions. The docking scores of all seven ligands are listed in Table 2. The resulting docked complexes were visualized and analyzed using Discovery Studio Visualizer v2024 (BIOVIA Dassault Systèmes) [19].

2.5. Molecular Dynamics Simulation

Molecular dynamics (MD) simulations were performed using GROMACS version 2025.1 to investigate the structural stability and dynamic behavior of the docked complexes formed between the Topo1B-DNA structure (1A36) and the three selected alkaloids (Berberine, Coptisine, and Epiberberine). These ligands were selected based on their docking affinity and binding orientation within the active site. Simulations were conducted to evaluate the conformational stability and persistence of protein–ligand interactions under explicit solvent conditions.

The protein structure (PDBID:1A36) was parameterized using the CHARMM36 force field. Ligand topology and parameter files for berberine, coptisine, and epiberberine were generated using SwissParam to ensure compatibility with the selected force field. Protonation states of ionizable residues were assigned at physiological pH (7.4) using PDB2PQR before system setup. Each receptor–ligand complex was examined for structural consistency before simulation. Each complex was placed in a cubic simulation box with a minimum solute–box distance of 10 Å and solvated using the CHARMM-modified TIP3P ex-

plicit water model. Counter ions (Na^+ and Cl^-) were added to neutralize the system, and the ionic strength was adjusted to 0.15 M to approximate physiological conditions. Energy minimization was performed using the steepest descent algorithm until the maximum force was reduced to below 1000 kJ mol^{-1} nm^{-1}. Equilibration was carried out in two stages: 500 ps (picoseconds) under the NVT ensemble at 300 K using the velocity-rescale thermostat, followed by 500 ps under the NPT ensemble at 1 bar using the Parrinello–Rahman barostat [20] [21]. Periodic boundary conditions were applied to the simulations. Long-range electrostatic interactions were treated using the Particle Mesh Ewald (PME) method, with a short-range cutoff of 1.2 nm. Production MD simulations were performed for 250 ns for each complex under NPT conditions at 300 K and 1 bar pressure. Trajectory coordinates were saved at 100 ps intervals for subsequent analysis [22]. Structural stability and conformational dynamics were evaluated using RMSD, RMSF, radius of gyration (Rg), solvent-accessible surface area (SASA), and hydrogen-bond analyses implemented in standard GROMACS tools.

2.6. MM/GBSA and MM/PBSA Binding Free Energy Analysis

The binding free energies of the receptor–ligand complexes were calculated using the Molecular Mechanics/Generalized Born Surface Area (MM/GBSA) and Molecular Mechanics/Poisson–Boltzmann Surface Area (MM/PBSA) methods implemented in gmx_MMPBSA v1.6.3, which integrates GROMACS trajectories with AmberTools for end-state free energy estimation [23], as presented in Supplementary Figures 5A and 5B. The binding free energy (ΔG_bind) was decomposed into molecular mechanical energy terms, including van der Waals (ΔEvdW) and electrostatic (ΔEele) interactions, together with solvation free energy contributions comprising polar (ΔG_polar) and nonpolar (ΔG_nonpolar) components, as expressed below:

$$\Delta G_{bind} = \Delta E_{vdW} + \Delta E_{ele} + \Delta G_{polar} + \Delta G_{nonpolar}$$

For MM/GBSA calculations, the polar solvation energy was determined using the Generalized Born implicit solvent model with the GB-Neck2 parameterization (igb = 5). For MM/PBSA calculations, the polar solvation contribution was computed using the Poisson–Boltzmann continuum solvent model. In both approaches, the nonpolar solvation energy was estimated from the solvent-accessible surface area using the LCPO method. Entropic contributions were not included because the calculations were performed for comparative evaluation of binding affinity [24]. A total of 1001 snapshots were extracted at uniform intervals from the equilibrated production trajectories of each protein–ligand complex. Free-energy calculations were performed separately for the complex, the receptor, and the ligands. The final binding free energy was obtained using the following equation:

$$\Delta G_{bind} = G_{complex} - (G_{receptor} + G_{ligand})$$

2.7. Total Decomposition (TDC) Energy Analysis

Per-residue total decomposition (TDC) analysis was performed using the gmx_MMPBSA tool, which integrates molecular mechanics energy terms with implicit solvent models to estimate binding free energies. Both MM/GBSA and MM/PBSA approaches were employed for residue-wise energy decomposition [25]. The binding free energy was decomposed into contributions from individual residues, including van der Waals, electrostatic, polar solvation, and nonpolar solvation. For MM/GBSA calculations, the polar solvation energy was determined using the Generalized Born (GB) model. In contrast, for MM/PBSA analysis, the polar solvation term was computed using the Poisson–Boltzmann (PB) continuum solvent model. The nonpolar solvation energy was estimated from the solvent-accessible surface area. The energetic components were calculated from the MD snapshots extracted at regular intervals from the equilibrated production trajectory. Time-dependent residue energy contributions were analyzed, and a moving average was applied to identify consistent energy trends. Separate decomposition analyses were conducted for each protein–ligand complex to identify key stabilizing residues and compare residue-level binding characteristics.

3. Results

3.1. DFT-based electronic descriptor analysis in comparison with camptothecin

Camptothecin (CPT), a prototypical topoisomerase I poison, is characterized by a moderate HOMO-LUMO gap (~3.0-3.6 eV), low chemical hardness, high electronic softness, and strong electrophilicity [27]. These features collectively facilitate charge-transfer interactions and stabilize the hTopo1B-DNA cleavage complex. In comparison, most of the studied ligands, berberastine, berberine, coptisine, epiberberine, jatrorrhizine, and palmatine, exhibited HOMO-LUMO gaps in the range of 2.608-3.015 eV (Fig.1), closely matching the electronic profile of CPT and indicating a favorable balance between stability and reactivity. Among these ligands, coptisine and epiberberine displayed the lowest HOMO-LUMO gaps (2.715 and 2.608 eV, respectively), indicating greater electronic softness and high chemical reactivity associated with enhanced charge-transfer capability and improved adaptability for intermolecular interactions, particularly π-π stacking and

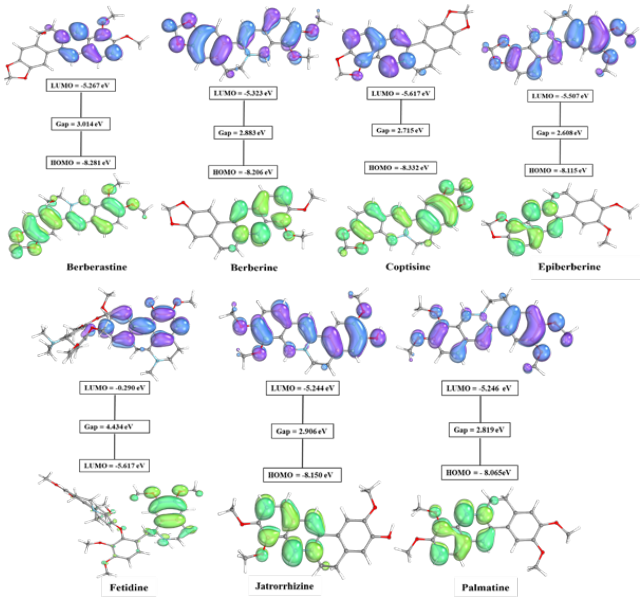


Fig. 1. HOMO and LUMO isosurface plots of the seven ligands with corresponding orbital energies and HOMO-LUMO gaps (ΔE, eV).

Table 1. Quantum Chemical Descriptors of seven ligands.

Descriptors	Berberastine	Berberine	Coptisine	Epiberberine	Fetidine	Jatrorrhizine	Palmatine
HOMO (eV)	−8.281	−8.206	−8.332	−8.115	−4.724	−8.150	−8.065
LUMO (eV)	−5.267	−5.323	−5.617	−5.507	−0.290	−5.244	−5.246
HOMO-LUMO gap, (ΔE)	3.014	2.883	2.715	2.608	4.434	2.906	2.819
Ionization potential, I (eV)	8.281	8.206	8.332	8.115	4.724	8.150	8.065
Electron affinity, A (eV)	5.267	5.323	5.617	5.507	0.290	5.244	5.246
Chemical hardness, η (eV)	1.507	1.442	1.358	1.304	2.217	1.453	1.410
Chemical softness, S ($eV^{)}$	0.664	0.693	0.736	0.767	0.451	0.688	0.709
Chemical potential, μ (eV)	−6.774	−6.795	−6.795	−6.811	−2.507	−6.697	−6.656
Electronegativity, χ (eV)	6.774	6.765	6.795	6.811	2.507	6.697	6.656
Electrophilicity index, ω (eV)	15.23	15.88	17.92	17.79	1.42	15.43	15.72

electronic stabilization at protein-DNA interfaces. Their electrophilicity indices (17.92 and 17.79 eV) (Table 1) further indicate a strong ability to accept electron density, supporting efficient charge-transfer interactions with DNA bases and the catalytic residues of hTopo1B.

Berberine, berberastine, jatrorrhizine, and palmatine also demonstrated substantial electrophilicity 15.23-15.88 eV together with large-magnitude negative chemical potentials −6.656 to −6.795 eV, consistent with favorable electron-accepting behavior and CPT-like interfacial stabilization properties. However, slightly less pronounced than those of coptisine and epiberberine, as shown in Fig.1. In contrast, fetidine exhibited a markedly different electronic profile, characterized by a large HOMO-LUMO gap 4.434 eV, high chemical hardness, low softness, and a very low electrophilicity index 0.42 eV. These features indicate reduced charge transfer capability and poor electronic compatibility with the CPT-like inhibition mechanism. Overall, the DFT analysis suggested that coptisine and epiberberine most closely resembled CPT in terms of electronic structure, followed by berberine, berberastine, jatrorrhizine, and palmatine, whereas fetidine showed minimal similarity. These results support the potential of berberine-type ligands, particularly coptisine and epiberberine, to function as CPT-like stabilizers of the hTopo1B-DNA cleavage complex (Table 1).

3.2. Molecular Mechanism Underlying Alkaloid-Mediated Interference with the hTopo1B Catalytic Cycle

3.2.1. DNA cleavage: Stabilization of the cleavage complex

Stabilization of the hTopo1B cleavage complex was observed for all seven compounds through camptothecin (CPT)-like DNA intercalation and π-π stacking interactions at the scissile site (Figures 2A-G). Berberine (Fig. 2A) adopts a similar cleavage-site intercalative pose, reinforced by hydrogen bonding with ARG362 and ARG364, and aromatic interactions with TYR268, residues known to participate in DNA positioning during catalysis. Coptisine (Fig. 2B) and epiberberine (Fig. 2C) exhibit the most pronounced CPT-like behavior, inserting their planar aromatic scaffolds between scissile DNA base pairs DA B:15/DT C:108-110, DT B:15-19, and DT C:108-110/DA B:15-18 and DT B:18, respectively, and forming stabilizing contacts with LYS746, resulting in deep burial at the protein-DNA interface. Berberastine (Fig. 2D) intercalates between DA B:5 and DA B:7, forming hydrogen bonds with DT C:118-119, thereby stabilizing the cleaved DNA intermediate. Fetidine (Fig. 2E) intercalates between DA B:13-14 and DT C:106-110, while extending toward the protein surface, suggesting a combined DNA and protein-mediated cleavage stabilization mechanism. Jatrorrhizine (Fig. 2F) stabilizes the cleavage through π-π stacking interactions with DG B:6 and hydrogen bonding with LYS216, VAL410, and LYS439, whereas palmatine (Fig. 2G) forms a mixed interaction network involving hydrogen bonds with ASN352, LYS425, and SER423, hydrophobic and π-alkyl interactions with PHE361, TYR426, MET428, ILE424, and ILE427, and strong aromatic stacking with DNA bases. Collectively, these DNA-dominant and DNA-protein cooperative interactions stabilize the covalent Topo1B-DNA cleavage complex by maintaining the persistent separation of cleaved DNA termini, as summarized in Table 2.

3.2.2. Controlled rotation: Restriction of DNA strand rotation

The restriction of controlled DNA rotation following cleavage is variably imposed by the seven compounds through protein anchoring and DNA-protein bridging interactions. Berberine (Fig. 2A) and berberastine (Fig.2D) partially restrict local DNA mobility through interactions with ARG362/ARG364 and LYS216, VAL410, thereby reducing strand flexibility near the catalytic pocket. Coptisine (Fig. 2B) and epiberberine (Fig. 2C) further constrain DNA swivel motion through stabilizing interactions with LYS746, which connects the cleavage site to the C-terminal domain and imposes additional conformational restraint. Fetidine (Fig. 2E) exhibits the strongest inhibition of controlled rotation by forming an extensive protein-DNA-ligand bridge involving hydrogen bonds with ASN745, GLN748, and ASN620, electrostatic interactions with LYS720 and ARG708, and aromatic stabilization by TYR744, resulting in rigid anchoring of the cleaved DNA strand. Jatrorrhizine (Fig. 2F) similarly restricts rotational motion through combined hydrogen bonding with LYS216, VAL410, and LYS439 and π-π stacking interactions with DG B:6 and DC B:8, whereas palmatine (Fig. 2G) limits DNA flexibility through hydrophobic enclosure and stabilizes protein contacts. Collectively, these interactions impede the rotational motion of DNA required for supercoil relaxation, consistent with the trends in control-

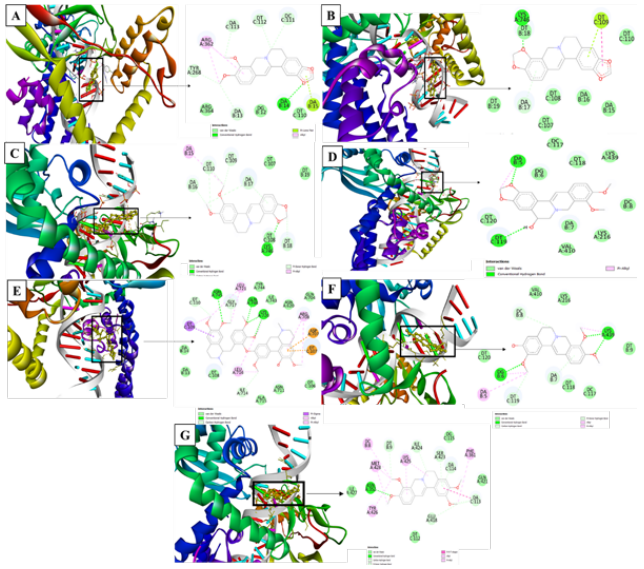


Fig. 2. Molecular docking analysis of (A) berberine, (B) coptisine, (C) epiberberine, (D) berberastine, (E) fetidine, (F) jatrorrhizine, and (G) palmatine binding within the human topoisomerase 1B active site.

led rotation inhibition summarized in Table 2.

3.2.3. DNA religation: Suppression of strand rejoining

Religation of the cleaved DNA strand requires precise realignment of DNA ends and reorganization of the catalytic pocket; all seven compounds uniformly suppressed these steps. Persistent DNA intercalation by berberastine, berberine, coptisine, epiberberine, fetidine, jatrorrhizine, and palmatine physically blocks realignment of the 3 ′- OH DNA terminus with the phosphotyrosyl linkage formed by the active-site tyrosine. Deep aromatic burial reduces solvent accessibility, whereas strong π-π stacking interactions maintain the ligands in locked conformations at the protein-DNA interface. Additional hydrogen bonding and electrostatic complementarity involving residues such as LYS216, ARG362, LYS439, TYR744, LYS746, and ASN745 further restrict active-site rearrangements required for strand resealing. As a result, DNA religation is inhibited, leading to prolonged accumulation of cleavage complexes and effective shutdown of hTopo1B catalytic activity. This behavior is consistent with a CPT-like hTopo1B poisoning mechanism and significant inhibition of religation, as supported by the docking scores and residue interactions presented in Table 2.

3.3. Structural Stability and Conformational Analysis

The backbone RMSD profiles of the 1A36 complexes with berberine (black), coptisine (orange), and epiberberine (blue) over a 250 ns simulation are shown in Fig. 3A. All systems exhibited an initial equilibration phase within the first ~50 ns, followed by gradual stabilization without persistent structural drift. The berberine complex

Table 2. Binding affinity of ligands to human topoisomerase 1B-DNA complex.

Ligand	DNA Cleavage Stabilization	Controlled Rotation Inhibition	DNA religation Suppression	Dominant Interaction Features	Docking scores	Residues Interaction
Coptisine	Strong	Strong	Strong	DNA Intercalation, DT H-bonds, π-π stacking	**−10.32**	LYS746; DAB15, DT B15,16,18,19; DT C108,109,110.
Epiberberine	Strong	Strong	Strong	π-π stacking, Lys 746/Arg contacts	**−10.53**	LYS746, DAB15, 16, 17, 18; DT C108, 109, 110; DT B18.
Berberastine	Strong	Moderate-strong	Strong	DNA-dominant binding, aromatic stacking	−9.57	LYS216,439; VAL410; DA B5,7; DT C118,119; DG B6.
Berberine	Strong	Moderate	Strong	Arg362/Arg364 H-bonds, DNA intercalation	**−9.88**	ARG362,364; TYR268; DA B13,14,15; DG B12; DT C110.
Fetidine	Strong	Very Strong	Very Strong	C-terminal and Core domain anchoring, deep burial	−9.33	ASN620,711, and 745; GLN704,748; LYS720; LEU716,721; ASP707; GLY717; ARG708; TYR744; ILE743; DA B:13-14 and DT C106-110
Jatrorrhizine	Moderate-strong	Strong	Strong	Lys216/Lys439 H-bonds, DNA stacking	−8.98	LYS216, 439; VAL410; DG B6; DA B5
Palmatine	Strong	Moderate	Strong	Core domain hydrophobic enclosure	−9.21	ASN352; ILE424, 427; GLU418; MET428; TYR426; LYS425; GLN421; PHE361; SER423; DA C113, 114; DC B8; DT B9.

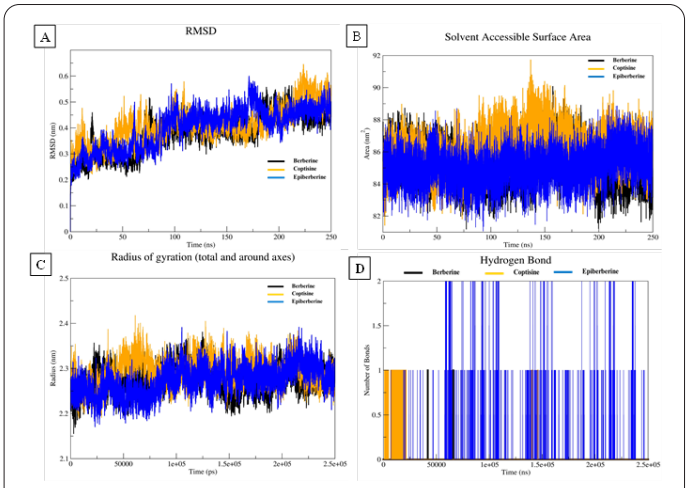


Fig. 3. Backbone trajectory profiles of 1A36 in complex with berberine(black), coptisine (orange), and epiberberine (blue) over 250 ns. (A) RMSD of backbone atoms showing structural stability of complexes with ligands. (B) Solvent accessible surface area (SASA) indicates changes in solvent exposure during the simulation. (C) The radius of gyration (Rg) reflects the compactness of the protein throughout the trajectory. (D) The number of intermolecular hydrogen bonds formed between the protein and ligands over time reflects the stability of the interactions.

showed the lowest mean RMSD (0.3797 ± 0.0763 nm, range: 0.0005–0.5629 nm), stabilizing around ~0.40–0.45 nm after ~100 ns. Coptisine displayed the highest deviation (0.4109 ± 0.0715 nm, range: 0.0005–0.6443 nm) and remained slightly elevated during the final 100 ns (~0.45–0.50 nm). Epiberberine showed an intermediate mean RMSD (0.3989 ± 0.0796 nm, range: 0.0005–0.5998 nm), with moderate fluctuations during the mid-simulation period before stabilization. Segment-wise analysis indicated that the largest conformational adjustments occurred during 0–150 ns, with epiberberine showing the highest intermediate increment (~0.1026 nm), followed by berberine (~0.093 nm) and coptisine (~0.0817 nm). During 150–250 ns, all systems fluctuated within a narrow range (~0.40–0.50 nm), indicating attainment of dynamic equilibrium.

SASA profiles (Fig. 3B) remained stable throughout the simulation, indicating that protein compactness was preserved. The mean SASA values were 85.2445 ± 1.0527 nm² for berberine, 86.1938 ± 1.2156 nm² for coptisine, and 85.0390 ± 1.0001 nm² for epiberberine. Coptisine exhibited the largest variation (10.2850 nm²), whereas epiberberine showed the lowest variation (7.8390 nm²), with berberine displaying intermediate behavior (8.8810 nm²). No progressive increase or decrease in SASA was observed, indicating that ligand binding did not induce structural expansion or unfolding.

The radius of gyration (Rg) analysis (Fig. 3C) further confirmed stable global compactness, with mean values of 2.2748 ± 0.0283 nm (berberine), 2.2921 ± 0.0293 nm (coptisine), and 2.2731 ± 0.0310 nm (epiberberine). Fluctuations remained confined within ~2.25–2.30 nm, and low standard deviations (~0.03 nm) indicated the absence of major structural expansion or collapse. Hydrogen bond analysis (Fig. 3D) revealed that the interactions were mostly transient. Berberine showed minimal hydrogen bonding, whereas coptisine formed occasional hydrogen bonds during the early simulation stages that diminished later. Epiberberine exhibited a higher frequency of hydrogen bonds, occasionally forming up to two simultaneous hydrogen bonds. However, persistent hydrogen bonding was not observed in any of the systems, suggesting that hydrophobic and aromatic interactions primarily stabilize the ligand-protein complexes.

3.4. Root Mean Square Fluctuations (RMSF) analysis

Figure 4 illustrates the Cα RMSF profiles of the 1A36 complexes, which exhibited low-to-moderate fluctuations across most residues, with mean RMSF values of 0.2003 ± 0.1228 nm (berberine), 0.1878 ± 0.1201 nm (coptisine), and 0.2115 ± 0.1579 nm (epiberberine). The majority of residues in each complex fluctuated below ~0.30–0.35 nm, indicating preservation of the structured protein core. Localized regions of high flexibility were primarily observed in the C-terminal region. In the berberine complex, elevated fluctuations were detected at residues 519–520 and 633 and were particularly pronounced within 642–689. Coptisine showed additional localized flexibility at residues 316–317, 375, and 434, along with a similarly high-fluctuation segment spanning 642-689 and minor peaks at 712–713. Epiberberine displayed the most pronounced C-terminal mobility, with a continuous high-fluctuation region extending from 656–693 and the highest maximum RMSF value (1.2718 nm), compared to berberine (1.0958 nm) and coptisine (0.9605 nm).

Despite these localized peaks, the core structural regions remained relatively rigid across all systems. Overall, the RMSF patterns indicate that ligand binding does not induce global destabilization of the protein, with flexibility largely confined to peripheral and terminal loop regions. At the same time, berberine and coptisine exhibit slightly lower overall fluctuations than epiberberine.

3.5. Molecular Mechanics-Based Free Energy Evaluation (MMGBSA/MMPBSA)

The binding free energies of the 1A36 complexes with berberine, coptisine, and epiberberine were estimated using both MM/GBSA and MM/PBSA approaches (Tables 3 and 4 and Fig S1.A and B). In the MM/GBSA analysis, epiberberine exhibited the most favorable total binding

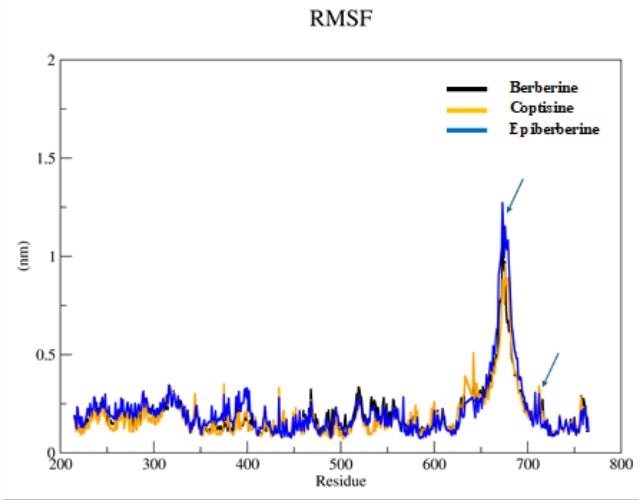


Fig. 4. RMSF profiles of 1A36 complexes with berberine (black), coptisine (orange), and epiberberine (blue) over 250 ns.

Table 3. MM/GBSA binding free-energy components (kcal/mol).

Component	Berberine	Coptisine	Epiberberine
VDWAALS	−09.17 ± 06.30	−04.49 ± 06.91	−21.17 ± 02.67
EEL	−626.83 ± 58.96	−554.01 ± 68.64	−471.96 ± 15.24
EGB	633.38 ± 61.86	557.13 ± 72.08	480.49 ± 15.49
ESURF	−00.90 ± 00.59	−00.42 ± 00.67	−01.48 ± 00.18
GGAS	−636.00 ± 63.99	−558.50 ± 74.81	−493.13 ± 16.23
GSOLV	632.48 ± 61.40	556.71 ± 71.50	479.01 ± 15.41
ΔG_total	−03.52 ± 03.35	−01.79 ± 03.96	−14.12 ± 02.33

Table 4. MM/PBSA binding free-energy components (kcal/mol).

Component	Berberine	Coptisine	Epiberberine
VDWAALS	−08.89 ± 06.09	−04.54 ± 07.37	−20.80 ± 03.20
EEL	−623.12 ± 60.87	−552.72 ± 70.85	−469.53 ± 14.95
EPB	621.99 ± 64.24	548.93 ± 74.48	473.31 ± 15.38
ENPOLAR	−01.02 ± 00.63	−00.47 ± 00.72	−01.84 ± 00.25
GGAS	−632.01 ± 65.69	−557.26 ± 77.44	−490.34 ± 16.43
GSOLV	620.97 ± 63.71	548.46 ± 73.83	471.47 ± 15.27
ΔG_total	−11.04 ± 2.53	−08.80 ± 04.04	−18.86 ± 02.68

free energy (ΔG_total = −14.12 ± 2.33 kcal/mol), which was markedly lower than that of berberine (−3.52 ± 3.35 kcal/mol) and coptisine (−1.79 ± 3.96 kcal/mol). All three complexes showed strong gas-phase electrostatic contributions (EEL), which were largely counterbalanced by polar solvation energy (EGB), resulting in modest net binding energies for berberine and coptisine. Notably, epiberberine exhibited a substantially stronger van der Waals contribution (−21.17 ± 2.67 kcal/mol) than those of berberine and coptisine, indicating enhanced hydrophobic stabilization within the binding pocket. The relatively smaller standard deviations observed for epiberberine further suggest greater energetic stability throughout the simulation trajectory.

Consistent trends were observed in the MM/PBSA calculations. Epiberberine again showed the most favorable total binding free energy (ΔG_total = −18.86 ± 2.68 kcal/mol), followed by berberine (−11.04 ± 2.53 kcal/mol) and coptisine (−8.80 ± 4.04 kcal/mol). Although berberine and coptisine exhibited stronger gas-phase electrostatic interactions (EEL), these were substantially offset by polar solvation penalties (EPB), thereby reducing their net-binding affinities. In contrast, epiberberine displayed a more favorable balance between van der Waals interactions (−20.80 ± 3.20 kcal/mol) and solvation effects, resulting in a significantly lower total free energy.

Overall, both MM/GBSA and MM/PBSA methods consistently ranked the binding affinities as Epiberberine > Berberine > Coptisine. The enhanced binding affinity of epiberberine is primarily attributed to stronger van der Waals interactions and a comparatively lower effective solvation penalty, indicating more stable accommodation within the 1A36 binding pocket. The agreement between GBSA and PBSA approaches strengthens the reliability of this energetic ranking.

3.6. Total Decomposition Energy Contribution (TDC) Energy Analysis

The per-residue free-energy decomposition analysis in Table 5 identified distinct stabilizing contributions from nucleotides and amino acids for each complex. In the Berberine-bound system, the primary favorable interactions were observed with DA B14 (−1.44 ± 1.54 kcal/

Table 5. Key residue-wise binding free energy contributions (kcal/mol) for Berberine, Coptisine, and Epiberberine obtained from per-residue MM/GBSA decomposition analysis.

Ligands	Nucleotide/Residue	Intercalated Drug Binding
Berberine	DAB14	−1.44±1.54
	DTC122	−1.09±0.77
	LEU166	−0.87±1.09
Coptisine	DTC118	−1.21±1.79
	DTC110	−1.41±0.77
	GLY201	−0.81±1.18
Epiberberine	DAB17	−1.71± 2.74
	DAB104	−0.76±2.11
	DTC118	−1.88±1.97
	GLY201	−0.53±0.97
	GLU179	−0.77±1.08

mol) and DT C122 (−1.09 ± 0.77 kcal/mol), along with a moderate contribution from LEU166 (−0.87 ± 1.09 kcal/mol), indicating involvement of both nucleic acid bases and nearby protein residues in stabilization. For Coptisine, the dominant contributions came from DT C118 (−1.21 ± 1.79 kcal/mol) and DT C110 (−1.41 ± 0.77 kcal/mol), with an additional contribution from GLY201 (−0.81 ± 1.18 kcal/mol), suggesting preferential interactions with thymine bases within the intercalation region. In contrast, epiberberine displayed stronger and more distributed residue-level stabilization, with significant contributions from DA B17 (−1.71 ± 2.74 kcal/mol) and DT C118 (−1.88 ± 1.97 kcal/mol), along with additional favorable interactions from DA B104 (−0.76 ± 2.11 kcal/mol), GLU179 (−0.77 ± 1.08 kcal/mol), and GLY201 (−0.53 ± 0.97 kcal/mol). The broader distribution and comparatively larger magnitude of residue contributions in the epiberberine complex are consistent with its more favorable total binding free energy, indicating enhanced stabilization within the intercalation site relative to berberine and coptisine. While docking highlights direct contacts in the representative binding pose, per-residue decomposition quantifies the average energetic contribution of residues across the entire molecular dynamics trajectory. Nevertheless, several residues identified in the docking analysis, including DA B14 (berberine), DT C110 (coptisine), and DA D17 (epiberberine), were also major energetic contributors, supporting consistency between the two approaches.

3.7. ADME and Drug-Likeness Analysis

As summarized in Table 6, the ADME drug-likeness analysis revealed that all seven investigated compounds, berberastine, berberine, coptisine, epiberberine, fetidine, jatrorrhizine, and palmatine, fully complied with Lipinski's Rule of Five, exhibiting molecular weights below 500 g/mol, zero rule violations, and favorable hydrogen-bond donor and acceptor counts. Fetidine was the sole exception, recording one Lipinski violation attributable to its markedly higher molecular weight (682.80 g/mol), which may restrict its oral bioavailability relative to the protoberberine congeners. All seven compounds demonstrated high predicted gastrointestinal (GI) absorption, indicating their potential for systemic exposure following oral administration. Except for fetidine, all compounds were predicted to be blood-brain barrier (BBB)-permeable and P-glycoprotein (P-gp) substrates. The latter represents a potential efflux liability that could limit intracellular drug accumulation in tumor cells and warrants consideration in future formulation strategies. Fetidine exhibited a notably higher synthetic accessibility score (6.06) than the other alkaloids, indicating greater synthetic complexity. This increased complexity may pose challenges for large-scale synthesis and structural optimization, potentially reducing its attractiveness as a lead candidate. The topological polar surface area (TPSA) values remained within the acceptable range for all compounds (40.80-91.32 $Å^2$), consistent with adequate membrane permeability. Lead-likeness assessment indicated that coptisine and jatrorrhizine met all lead-likeness criteria compared with other compounds; such violations are common among bioactive natural products and do not necessarily hinder further development, particularly when favorable binding and pharmacokinetic characteristics are observed. Cytochrome P450 profiling indicated that most protoberberine alkaloids are inhibitors of CYP1A2, CYP2D6, and CYP3A4, suggesting potential metabolic drug-drug interactions that should be carefully evaluated in future in vivo studies. Notably, all compounds yielded zero PAINS alerts, and their synthetic accessibility scores (2.96-3.63) indicate the feasibility of laboratory synthesis and structural optimization. Collectively, the predicted ADME profiles support the drug-like properties of the protoberberine alkaloids, particularly coptisine, epiberberine, berberine, berberastine, jatrorrhizine, and palmatine, as viable lead candidates, warranting further preclinical investigation.

4. Discussion

The present study provides convergent evidence that protoberberine alkaloids, particularly berberine, coptisine, and epiberberine, act as camptothecin (CPT)-like poisons of human topoisomerase 1 (hTopo1B) by stabilizing the cleavage complex and disrupting the catalytic cycle. Topoisomerase 1 inhibitors exert cytotoxicity primarily through interfacial inhibition, in which planar ligands intercalate at the protein-DNA interface, trap the covalent hTopo1B-DNA complex, prevent religation, and cause lethal damage. This mechanism is well established for CPT and its clinical derivatives and remains the principal framework for hTopo1B-targeted anticancer drug discovery [26]. The present findings indicate that certain protoberberine alkaloids may replicate and, in some aspects, enhance the key elements of this canonical inhibition mechanism.

4.1. Electronic structure determinants of CPT-like activity

DFT descriptors revealed that most of the investigated alkaloids exhibit electronic properties closely resembling those of CPT [27]. The observed HOMO-LUMO gaps for berberastine, berberine, coptisine, epiberberine, jatrorrhizine, and palmatine (2.608-3.015 eV) are consistent with frontier orbital energy differences that favor intermolecular charge-transfer interactions, as described in molecular orbital-based analyses of donor-acceptor systems [28]. These moderate band gaps indicate balanced molecular reactivity, which is advantageous for stabilizing transient enzymatic intermediates, such as the hTopo1B-DNA cleavage complex [29]. These electronic features facilitate π-π stacking with DNA bases and electrostatic complementarity within the catalytic pocket, key determinants of TOPO1 poison activity. The particularly low energy gaps and high electrophilicity of coptisine and epiberberine suggest enhanced ability to accept electron density from nucleobases and catalytic residues, thereby stabilizing the cleavage complex. Electronic softness is correlated with increased intermolecular interaction potential and binding adaptability in DNA-targeting drugs, supporting the superior CPT-like behavior predicted for these ligands. In contrast, fetidine exhibited a large HOMO-LUMO gap and high hardness, indicating reduced polarizability and weaker interfacial interactions, consistent with its diminished mechanistic compatibility.

4.2. Interference with the hTopo1B catalytic cycle

Molecular docking demonstrated that all ligands stabilized the cleavage complex through DNA intercalation and protein-assisted anchoring, recapitulating the canonical CPT-like binding mode. The strongest effects observed for coptisine and epiberberine at the scissile site, along

Table 6. Pharmacokinetic, ADME, and drug-likeness of the studied ligands.

	Berberastine	**Berberine**	**Coptisine**	**Epiberberine**	**Fetidine**	**Jatrorrhizine**	**Palmatine**
Formula	$C_{20}H_{18}NO^{+5}$	$C_{20}H_{18}NO^{+4}$	$C_{19}H_{14}NO^{+4}$	$C_{20}H_{18}NO^{+4}$	$C_{40}H_{46}N_2O_8$	$C_{20}H_{20}NO^{+4}$	$C_{21}H_{22}NO^{+4}$
Molecular weight	352.36 g/mol	336.4 g/mol	320.3 g/mol	336.36 g/mol	682.80 g/mol	338.4 g/mol	351.4 g/mol
Num. heavy atoms	26	25	24	25	50	25	26
Num. arom. heavy atoms	16	16	18	16	24	16	16
Fraction Csp3	0.25	0.25	0.21	0.25	0.40	0.25	0.29
Num. rotatable bonds	2	2	0	2	10	3	4
Num. H-bond acceptors	5	4	4	4	10	4	4
Num. H-bond donors	1	0	0	0	1	1	0
Molar Refractivity	96.04	94.87	87.95	94.87	200.00	97.33	101.80
TPSA	61.03 Å^2	40.80 Å^2	40.80 Å^2	40.80 Å^2	91.32 Å^2	51.80 Å^2	40.80 Å^2
GI absorption	High	High	High	High	High	High	High
BBB permeant	Yes	Yes	Yes	Yes	No	Yes	Yes
P-gp substrate	Yes	Yes	Yes	Yes	No	Yes	Yes
CYP1A2 inhibitor	Yes	Yes	Yes	Yes	No	Yes	No
CYP2C19 inhibitor	Yes	No	No	No	No	No	No
CYP2C9 inhibitor	No	No	No	No	No	No	No
CYP2D6 inhibitor	Yes	Yes	No	Yes	No	Yes	Yes
CYP3A4 inhibitor	Yes	Yes	Yes	Yes	No	Yes	Yes
Log Kp (skin permeation)	-6.67 cm/s	-5.78 cm/s	-5.78 cm/s	-5.78 cm/s	-5.96 cm/s	-5.94 cm/s	-5.79 cm/s
Lipinski #Violations	Yes;0	Yes;0	Yes;0	Yes;0	Yes;1	Yes;0	Yes;0
Ghose #Violations	Yes	Yes	Yes	Yes	No	Yes	Yes
Veber #Violations	Yes	Yes	Yes	Yes	Yes	Yes	Yes
Egan #Violations	Yes	Yes	Yes	Yes	Yes	Yes	Yes
Muegge #Violations	Yes	Yes	Yes	Yes	No	Yes	Yes
Bioavailability Score	0.55	0.55	0.55	0.55	0.55	0.55	0.55
PAINS #alerts	0 alert	0 alert	0 alert	0 alert	0 alert	0 alert	0 alert
Brenk #alerts	1 alert	1 alert	1 alert	1 alert	0 alert	1 alert	1 alert
Leadlikeness #Violations	No	No	Yes	No	No	Yes	No
synthetic accessibility	3.63	3.14	2.96	3.14	6.06	3.06	3.18
Total clearance	1.132	1.27	1.28	1.27	0.977	1.22	1.24
Renal OCT2	No	No	Yes	Yes	No	No	No

with interactions with the C-terminal domain of LYS746, suggest efficient trapping of the covalent intermediate. Stabilization of this intermediate prevents controlled rotation of the cleaved strand and blocks religation, the two subsequent steps of the Topo1 catalytic cycle [30]. Berberine and berberastine also adopted stable intercalative poses, although their interaction networks showed greater contributions from catalytic residues such as ARG362 and ARG364, which are involved in DNA positioning within the active site. Jatrorrhizine and palmatine exhibited similar DNA-dominant binding modes, supported by additional hydrogen bonding and hydrophobic contacts with surrounding residues, which contributed to the stabilization of the cleavage intermediate. This trapping converts an essential enzyme into a DNA-damaging lesion, a hallmark of Topo1B poisons. Protein-DNA-ligand bridging interactions, particularly those involving C-terminal domain residues, further restrict DNA swivel motion, explaining the observed inhibition of controlled rotation [31]. Persistent intercalation and steric hindrance at the 3'-OH alignment sites rationalize the suppression of religation across all compounds, leading to the accumulation of cleavage complexes and catalytic shutdown.

4.3. Dynamic stability of ligand-hTopo1B-DNA complexes

Molecular dynamics simulations confirmed stable accommodation of berberine, coptisine, and epiberberine within the binding site. RMSD stabilization after equilibration indicates attainment of conformational equilibrium, whereas limited SASA and Rg fluctuations demonstrate the preservation of global compactness without protein unfolding. Per-residue RMSF profiles demonstrated that ligand association preserves the stability of the structured catalytic core, while conformational flexibility remains confined to intrinsically dynamic terminal regions. Such localized stabilization without global structural rearrangement is characteristic of an effective Topo1 poison, which acts by reinforcing the protein-DNA interface rather than perturbing the enzyme's overall fold [32]. The predominance of transient hydrogen bonds and reliance on hydrophobic and aromatic interactions are also consistent with the binding characteristics of interfacial inhibitors, in which π-stacking and van der Waals contacts dominate over persistent polar interactions [33].

4.4. Energetic basis of binding affinity

MM/GBSA and MM/PBSA analyses consistently ranked binding affinity as epiberberine > berberine > coptisine. The superior affinity of epiberberine arises primarily from strong van der Waals contributions and a favorable balance between electrostatic attraction and solvation penalties. Hydrophobic stabilization within the intercalation pocket is a recognized determinant of Topo1 poison potency, as it prolongs the residence time at the cleavage site [34]. Per-residue decomposition further revealed that epiberberine engages a broader network of stabilizing DNA bases and protein residues, which explains its lower total free energy and suggests more effective interfacial trapping. However, direct experimental evidence that epiberberine acts as a hTopo1B poison is currently lacking in the literature. Although berberine and coptisine have been shown to act against camptothecin-resistant topoisomerase I mutants in cellular assays [35], no equivalent *in vitro* validation of epiberberine has been reported. Therefore, the present computational findings serve as a basis for prioritizing epiberberine in future in vitro and cell-based studies.

4.5. Residue-level interaction patterns

Per-residue free-energy decomposition analysis provided additional mechanistic insights into ligand stabilization at the intercalation site [36]. In the berberine complex, key stabilizing contributions were associated with DNA bases such as DA14 and DT122, indicating a primarily nucleic acid-driven interaction pattern. Coptisine preferentially stabilized the interaction region, particularly DT110 and DT118, through interactions with thymine bases, suggesting a localized DNA-binding mode. In contrast, the epiberberine complex displayed a broader distribution of stabilizing contributions involving both nucleotides and protein residues, including DA17, DT118, GLU179, and GLY201. The distributed interaction network likely contributes to the enhanced energetic stability of epiberberine.

4.6. Pharmacokinetic feasibility

ADME prediction indicated that most ligands satisfied key drug-like criteria, including oral absorption potential and acceptable molecular properties [37]. High gastrointestinal absorption and moderate polar surface areas support systemic bioavailability [38]; predicted CYP interactions highlight possible metabolic considerations typical of aromatic alkaloids [39]. The absence of major PAINS alerts and the presence of reasonable synthetic accessibility further support their candidacy as lead compounds [40]. Most protoberberine alkaloids generated a single Brenk alert associated with their aromatic heterocyclic scaffold, indicating a potential area for future medicinal chemistry optimization rather than a major liability. However, P-glycoprotein substrate status suggests potential efflux liability, a known challenge for many Topo1 inhibitors [41]. Although fetidine had a higher molecular weight and one Lipinski violation, the remaining protoberberine derivatives exhibited pharmacokinetic profiles consistent with those of drug-like small molecules.

5. Conclusion

Taken together, the computational analyses indicate that protoberberine alkaloids can reproduce multiple structural and electronic features associated with CPT-like inhibition of human topoisomerase 1B. The favorable interactions at the Topo1B-DNA interface support their potential to serve as Topo1B-poisoning agents. Among the investigated compounds, epiberberine was the most promising candidate, exhibiting the most favorable binding free energy, a broad distribution of stabilizing interactions, and sustained structural stability during long-timescale simulations. Coptisine and berberine also demonstrated significant inhibitory potential, although their binding energies and interaction networks were comparatively less extensive. These findings indicate that protoberberine alkaloids can mimic and enhance the canonical camptothecin-mediated inhibition mechanism by stabilizing the Topo1B-DNA cleavage complex and disrupting the enzyme catalytic cycle. As a result, these compounds represent promising scaffolds for the rational design of next-generation topoisomerase I inhibitors.

Study limitations
Further experimental studies, including *in vitro* hTopo1 relaxation and DNA cleavage assays, evaluation of cellular cytotoxicity, and structural validation experiments, are necessary to validate the computational predictions, confirm the proposed mechanism of action, and assess the therapeutic potential of these compounds.

Conflict of interest
There is no conflict of interest.

Consent of publication
The authors read and approved the final manuscript for publication.

Author contributions
J.B.D. Conceptualization, Writing-original draft, Validation, Investigation, Software, Supervision. **M.B.D.** Validation, Software, Writing-review & editing, **B.C.S.** Writing, original draft, Validation, Formal analysis. **A.C.** Validation, Writing, review & editing. **S.J.** Formal analysis & validation, Writing-review.

Availability of data and material
The original contributions presented in this study are included in the supplementary materials. Further inquiries can be directed to the corresponding author.

Funding
This research did not receive any specific grant from funding agencies in the public, commercial, or not-for-profit sectors.

Generative AI Statement
The author declares that generative AI (artificial intelligence) tools, including Grammarly & QuillBot, were used to enhance the language & clarity of this work. The author takes full responsibility for the accuracy & integrity of the content.

References

1. Sung H, Ferlay J, Siegel RL, Laversanne M, Soerjomataram I, Jemal A, Bray F. Global Cancer Statistics 2020: GLOBOCAN Estimates of Incidence and Mortality Worldwide for 36 Cancers in 185 Countries. CA Cancer J Clin 2021; 71(3): 209-249. doi: 10.3322/caac.21660
2. Pommier Y. Topoisomerase I inhibitors: camptothecins and beyond. Nat Rev Cancer 2006; 6(10): 789-802. doi: 10.1038/nrc1977
3. Pommier Y, Sun Y, Huang SN, Nitiss JL. Roles of eukaryotic topoisomerases in transcription, replication, and genomic stability. Nat Rev Mol Cell Biol 2016; 17(11): 703-721. doi: 10.1038/nrm.2016.111
4. Soren BC, Dasari JB, Ottaviani A, Iacovelli F, Fiorani P. Topoisomerase IB: a relaxing enzyme for stressed DNA. Cancer Drug Resist 2020; 3(1): 18-25. doi: 10.20517/cdr.2019.106
5. Ulukan H, Swaan PW. Camptothecins: a review of their chemotherapeutic potential. Drugs 2002; 62(14): 2039-2057. doi: 10.2165/00003495-200262140-00004
6. Thomas A, Pommier Y. Targeting topoisomerase I in the Era of Precision Medicine. Clin Cancer Res 2019; 25(22): 6581-6589. doi: 10.1158/1078-0432.CCR-19-1089
7. Chen Z, Liu M, Wang N, Xiao W, Shi J. Unleashing the Potential of Camptothecin: Exploring Innovative Strategies for Structural Modification and Therapeutic Advancements. J Med Chem 2024; 67(11): 3244-3273. doi: 10.1021/acs.jmedchem.3c02115
8. Gezici S, Şekeroğlu N. Current Perspectives in the Application of Medicinal Plants Against Cancer: Novel Therapeutic Agents. Anticancer Agents Med Chem 2019; 19(1): 101-111. doi: 10.2174/1871520619666181224121004
9. Grycová L, Dostál J, Marek R. Quaternary protoberberine alkaloids. Phytochemistry 2007; 68(2): 150-175. doi: 10.1016/j.phytochem.2006.10.004
10. Ortiz LM, Lombardi P, Tillhon M, Scovassi AI. Berberine, an epiphany against cancer. Molecules 2014; 19(8): 12349-12367. doi: 10.3390/molecules190812349
11. Vieira S, Castelli S, Falconi M, Takarada J, Fiorillo G, Buzzetti F, Lombardi P, Desideri A. Role of 13-(di)phenylalkyl berberine derivatives in the modulation of the activity of human topoisomerase IB. Int J Biol Macromol 2015; 77: 68-75. doi: 10.1016/j.ijbiomac.2015.02.051
12. Maiti M, Kumar GS. Molecular aspects of the interaction of protoberberine, benzophenanthridine, and aristolochia group of alkaloids with nucleic acid structures and biological perspectives. Med Res Rev 2007; 27(5): 649-695. doi: 10.1002/med.20087
13. He L, Zhong Z, Chen M, Liang Q, Wang Y, Tan W. Current Advances in Coptidis Rhizoma for Gastrointestinal and Other Cancers. Front Pharmacol 2022; 12: 775084, 1-35. doi: 10.3389/fphar.2021.775084
14. Pettersen EF, Goddard TD, Huang CC, Meng EC, Couch GS, Croll TI, Morris JH, Ferrin TE. UCSF ChimeraX: Structure visualization for researchers, educators, and developers. Protein Sci 2021; 30(1): 70-82. doi:10.1002/pro.3943
15. Morris GM, Huey R, Lindstrom W, Sanner MF, Belew RK, Goodsell DS, Olson AJ. AutoDock4 and AutoDockTools4: Automated docking with selective receptor flexibility. J Comput Chem 2009; 30(16): 2785-2791. doi: 10.1002/jcc.21256
16. Hanwell MD, Curtis DE, Lonie DC, Vandermeersch T, Zurek E, Hutchison GR. Avogadro: an advanced semantic chemical editor, visualization, and analysis platform. J Cheminform 2012; 4(1): 17. doi: 10.1186/1758-2946-4-17
17. Neese F. Software Update: The ORCA Program System—Version 6.0. WIREs Comput Mol Sci 2025; 15: e70019. doi: 10.1002/wcms.70019
18. Laskowski R, MacArthur MW, Moss DS, Thornton JM. PROCHECK: a program to check the stereochemical quality of protein structures. J Appl Crystallogr 1993; 26(2): 283-291. doi:10.1107/S0021889892009944
19. BIOVIA Discovery Studio Visualizer v21.1.0.20298, 2023. Available from: https://discover.3ds.com/discovery-studio-visualizer-download (accessed on 20-4-2025)
20. Abraham MJ, Murtola T, Schulz R, Páll S, Smith JC, Hess B, Lindahl E. GROMACS: High-performance molecular simulations through multi-level parallelism from laptops to supercomputers. SoftwareX 2015; 1: 19-25. doi: 10.1016/j.softx.2015.06.001
21. Ke Q, Gong X, Liao S, Duan C, Li L. Effects of thermostats/barostats on physical properties of liquids by molecular dynamics simulations. J Mol Liq 2022; 365: 120116. doi: 10.1016/j.molliq.2022.120116
22. Valdés-Tresanco MS, Valdés-Tresanco ME, Valiente PA, Moreno E. gmx_MMPBSA: A New Tool to Perform End-State Free Energy Calculations with GROMACS. J Chem Theory Comput 2021; 17(10): 6281-6291. doi: 10.1021/acs.jctc.1c00645
23. Miller BR 3rd, McGee TD Jr, Swails JM, Homeyer N, Gohlke H, Roitberg AE. MMPBSA.py: An Efficient Program for End-State Free Energy Calculations. J Chem Theory Comput 2012; 8(9): 3314-3321. doi: 10.1021/ct300418h

24. Kollman PA, Massova I, Reyes C, Kuhn B, Huo S, Chong L, Lee M, Lee T, Duan Y, Wang W, Donini O, Cieplak P, Srinivasan J, Case DA, Cheatham TE. Calculating Structures and Free Energies of Complex Molecules: Combining Molecular Mechanics and Continuum Models. Acc Chem Res 2000; 33(12): 889-897. doi: 10.1021/ar000033j
25. Genheden S, Ryde U. The MM/PBSA and MM/GBSA methods to estimate ligand-binding affinities. Expert Opin Drug Discov 2015; 10(5): 449-461. doi: 10.1517/17460441.2015.1032936
26. Yakkala PA, Penumallu NR, Shafi S, Kamal A. Prospects of Topoisomerase Inhibitors as Promising Anti-Cancer Agents. Pharmaceuticals 2023; 16(10): 1456. doi: 10.3390/ph16101456
27. Lai CH, Chang CC, Weng YL, Chuang TH. Synthesis, Experimental, and Density Functional Theory (DFT) Studies on the Solubility of Camptothecin Derivatives. Molecules 2018; 23(12): 3170. doi:10.3390/molecules23123170
28. Lin Z, Su H, Huang W, Zhang X, Zhang G. 2D-Graph of intermolecular interactions predicts radical character of anion-π* type charge-transfer complexes. RSC Adv 2024; 14(6): 3771-3775. doi: 10.1039/d3ra07729b
29. Ivanova BB, Spiteller M. Experimental and theoretical spectroscopic and structural study of A-ring substituted camptothecins. J Mol Struct 2012; 1012: 189-197. doi: 10.1016/j.molstruc.2012.01.001
30. Talukdar A, Kundu B, Sarkar D, Goon S, Mondal MA. Topoisomerase I inhibitors: Challenges, progress, and the road ahead. Eur J Med Chem 2022; 236: 114304. doi: 10.1016/j.ejmech.2022.114304
31. Takahashi DT, Gadelle D, Agama K, Kiselev E, Zhang H, Yab E, Petrella S, Forterre P, Pommier Y, Mayer C. Topoisomerase I (TOP1) dynamics: conformational transition from open to closed states. Nat Commun 2022; 13(1): 59. doi:10.1038/s41467-021-27686-7
32. Madeddu F, Di Martino J, Pieroni M, Del Buono D, Bottoni P, Botta L, Castrignanò T, Saladino R. Molecular Docking and Dynamics Simulation Revealed the Potential Inhibitory Activity of New Drugs against Human Topoisomerase I. Int J Mol Sci 2022; 23(23): 14652. doi: 10.3390/ijms232314652
33. Pommier Y, Marchand C. Interfacial inhibitors: targeting macromolecular complexes. Nat Rev Drug Discov 2011; 11(1): 25-36. doi: 10.1038/nrd3404
34. Song Y, Cushman M. The binding orientation of a norindenoisoquinoline in the topoisomerase I-DNA cleavage complex is primarily governed by pi-pi stacking interactions. J Phys Chem B 2008; 112(31): 9484-9489. doi: 10.1021/jp8005603
35. Inoue N, Terabayashi T, Takiguchi-Kawashima Y, Fujinami D, Matsuoka S, Kawano M, Tanaka K, Tsumura H, Ishizaki T, Narahara H, Kohda D, Nishida Y, Hanada K. The benzylisoquinoline alkaloids, berberine and coptisine, act against camptothecin-resistant topoisomerase I mutants. Sci Rep 2021; 11(1): 7718. doi: 10.1038/s41598-021-87344-2
36. Wang E, Sun H, Wang J, Wang Z, Liu H, Zhang JZH, Hou T. End-Point Binding Free Energy Calculation with MM/PBSA and MM/GBSA: Strategies and Applications in Drug Design. Chem Rev 2019; 119(16): 9478-9508. doi: 10.1021/acs.chemrev.9b00055
37. Lipinski CA, Lombardo F, Dominy BW, Feeney PJ. Experimental and computational approaches to estimate solubility and permeability in drug discovery and development settings. Adv Drug Deliv Rev 2001; 46(1-3): 3-26. doi:10.1016/s0169-409x(00)00129-0
38. Ertl P, Rohde B, Selzer P. Fast calculation of molecular polar surface area as a sum of fragment-based contributions and its application to the prediction of drug transport properties. J Med Chem 2000; 43(20): 3714-3717. doi:10.1021/jm000942e
39. Daina A, Michielin O, Zoete V. SwissADME: a free web tool to evaluate pharmacokinetics, drug-likeness and medicinal chemistry friendliness of small molecules. Sci Rep 2017; 7: 42717. doi:10.1038/srep42717
40. Baell JB, Holloway GA. New substructure filters for removal of pan assay interference compounds (PAINS) from screening libraries and for their exclusion in bioassays. J Med Chem 2010; 53(7): 2719-2740. doi:10.1021/jm901137j
41. Callaghan R, Luk F, Bebawy M. Inhibition of the multidrug resistance P-glycoprotein: time for a change of strategy? Drug Metab Dispos 2014; 42(4): 623-631. doi:10.1124/dmd.113.056176